

## Elliptical x-ray microprobe mirrors by differential deposition

Gene E. Ice,<sup>a)</sup> Jin-Seok Chung, and Jonathan Z. Tischler  
Oak Ridge National Laboratory, Bethel Valley Road, Oak Ridge, Tennessee 37831-6118

Andrew Lunt  
Beamline Technology, 1683 West Grant Road, Suite 105, Tucson, Arizona 85745

Lahsen Assoufid  
Argonne National Laboratory, 970 S. Cass Avenue, Argonne, Illinois 60439

(Received 29 December 1999; accepted for publication 27 March 2000)

A differential coating method is described for fabricating high-performance x-ray microfocusing mirrors. With this method, the figure of ultrasmooth spherical mirrors can be modified to produce elliptical surfaces with low roughness and low figure errors. Submicron focusing is demonstrated with prototype mirrors. The differential deposition method creates stiff monolithic mirrors which are compact, robust, and easy to cool and align. Prototype mirrors have demonstrated gains of more than  $10^4$  in beam intensity while maintaining submilliradian divergence on the sample. This method of producing elliptical mirrors is well matched to the requirements of an x-ray microdiffraction Kirkpatrick–Baez focusing system. © 2000 American Institute of Physics.  
[S0034-6748(00)01607-5]

### I. INTRODUCTION

With the recent availability of high-brilliance third-generation synchrotron sources, there is an immediate need for efficient x-ray microfocusing optics. Efforts are currently underway to produce microfocusing optics by a variety of means including tapered capillaries, Bragg–Fresnel optics, Fresnel Zone plates, compound refractive lenses and Kirkpatrick–Baez (K–B) mirrors.<sup>1</sup> Total external specular-reflecting (K–B) mirrors are particularly attractive for microfocusing broad bandpass or tunable radiation since they are inherently nondispersive. K–B optics utilize two concave mirrors at glancing angle to collect and focus x rays in both vertical and horizontal axis (Fig. 1). K–B mirrors were pioneered in the late 1940's,<sup>2</sup> but are being revolutionized by modern materials and processing methods.

In the x-ray regime, K–B optics can be made from total-external-reflection mirrors, multilayer mirrors or a combination of total-external and multilayer mirrors.<sup>3</sup> Total external reflection x-ray optics are efficient x-ray analogs to total internal reflection optics commonly used with visible light. However, at x-ray wavelengths the index of refraction of materials is less than 1 and the deviation from unity is roughly proportional to the electron density

$$n \sim 1 - \delta + i\beta. \quad (1)$$

Here  $1 - \delta$  is the real and  $i\beta$  is the imaginary index of refraction. In the hard x-ray regime,  $\delta \sim 10^{-5} - 10^{-6}$ . Because  $n < 1$  x rays bend away from the normal when entering dense materials whereas visible light bends toward the normal. Nearly 100% specular reflectivity occurs when the glancing angle,  $\theta$ , is below a so-called critical angle  $\theta_c$ . For a dense metal like palladium, the critical angle depends on

x-ray energy as  $\theta_c \sim 0.06/E_{\text{keV}}$  and the evanescent wave penetrates  $\sim 15 - 60 \text{ \AA}$  for  $\theta = 3 \text{ mrad}$  and  $h\nu = 5 - 20 \text{ keV}$  (Fig. 2). High reflectivity is therefore achieved if  $E < 20 \text{ keV}$  and  $\theta < 0.003 \text{ rad}$ . For x-ray microdiffraction  $\sim 25 \text{ keV}$  is a useful upper energy and therefore Pd with a K-absorption edge at 24.35 keV is an excellent surface material.

A major obstacle to the use of K–B mirrors is the need to create elliptical surfaces with x-ray quality figure and roughness. Surface figure perfection is required to focus x rays to a small focal spot. Surface roughness perfection is required to prevent diffuse scattering of x rays. For microfocus mirrors, submicroradian figure perfection and surface roughness of less than  $\sim 3 \text{ \AA}$  is desirable.<sup>4</sup>

Advances in mirror manufacturing have recently made it possible to fabricate x-ray mirrors with a few angstroms root-mean-square (rms) roughness and with submicroradian deviations from ideal spherical or flat figure. However, no known technique exists for polishing elliptical mirrors to x-ray quality surface roughness. As a result, sophisticated bending techniques are used to shape x-ray quality flats to ellipses.<sup>5,6</sup> These methods have successfully produced submicron x-ray beams, but are sensitive to the bender adjustment, are difficult to cool, and are bulky compared to monolithic mirrors. Because of their additional bulk, benders become increasingly less attractive with stronger demagnification (decreased focal length).

In this article we describe a new approach for the production of elliptical K–B mirrors. With this approach, an ultrasmooth Au layer is differentially deposited on a cylindrical substrate to modify the cylinder to an ellipse. This approach was first suggested by Cai *et al.*<sup>7</sup> and is similar to ion milling modification of mirror figure which has been used to perfect the figure of high-performance astronomical laser and x-ray mirrors.<sup>8</sup>

<sup>a)</sup>Electronic mail: icege@oml.gov

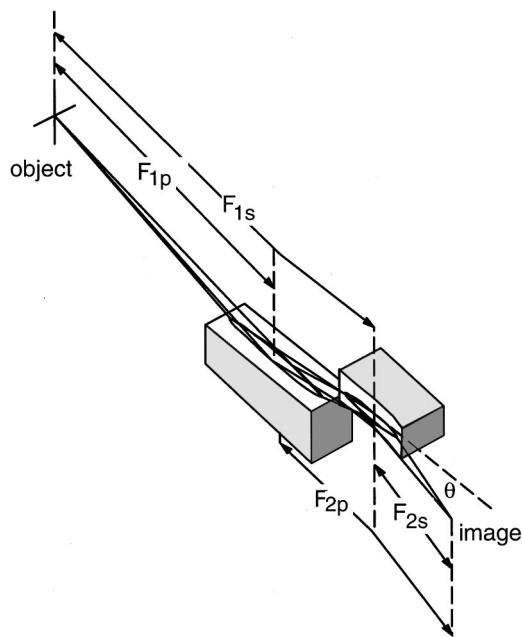


FIG. 1. K-B focusing scheme. The crossed mirrors focus the x-ray beam in orthogonal directions. The object and image distances are labeled  $F_1$  and  $F_2$  and are distinguished for the primary and secondary mirrors by a “p” or “s.”

## II. FIGURE MODIFICATION FROM SPHERICAL TO ELLIPTICAL

At large demagnifications elliptical optics are essential for efficient focusing and preservation of beam brilliance (photons/s/eV/ $\mu\text{rad}^2/\mu\text{m}^2$ ). For example, Howells and Hastings<sup>9</sup> have considered the case of microfocusing with cylindrical optics. They show that spherical aberrations cause a point source to be imaged into a blur in the scattering plane with dimensions determined by the distance to the source,  $F_1$ , the opening angle,  $2\gamma$ , of the intercepted radiation and the magnification,  $M$ :

$$Y_{\text{spherical}} = 3F_1(1+M)\gamma^2/4M\theta. \quad (2)$$

At the Advanced Photon Source (APS), the type A undulators have typical full width at half maximum (FWHM) horizontal and vertical source sizes of  $\sim 720 \times 65 \mu\text{m}^2$ .<sup>10</sup> Based

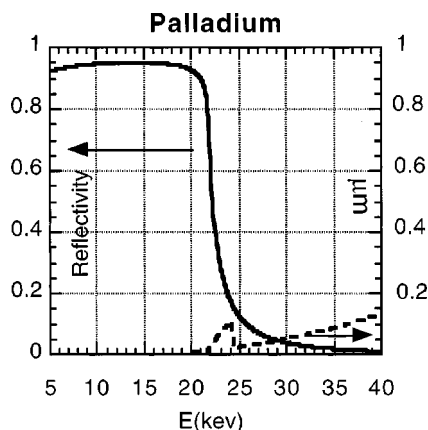


FIG. 2. Reflectivity and penetration depth of x rays from Pd as a function of energy at 3 mrad glancing angle. The beam penetrates only about 15–50 Å into the Pd surface below 20 keV.

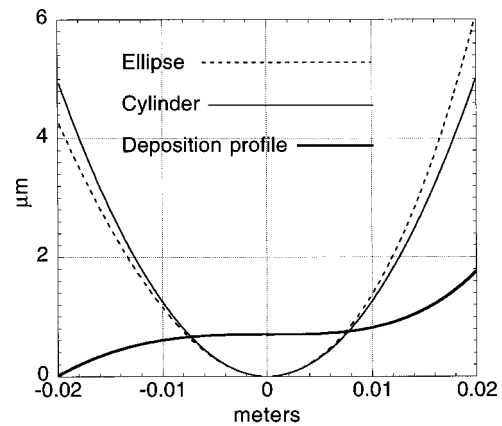


FIG. 3. Figure for an ideal ellipse compared to its cylindrical approximation. The deposition profile transforms the cylindrical approximation into the ideal ellipse. The values shown are for  $F_2 \sim 35$  m, and  $\theta = 0.003$  rad.

on the required geometrical demagnification with an  $\sim 30$  m object distance ( $F_1$ ), Eq. (2) places a limit on the vertical and horizontal acceptance  $2\gamma_v$  and  $2\gamma_h$  that can be focused by meridional-focusing cylindrical mirrors to submicron dimensions. For one micron focusing, the horizontal acceptance  $2\gamma_h < 0.86 \mu\text{rad}$  ( $26 \mu\text{m}$  at 30 m from source). In the vertical direction submicron focusing with cylindrical optics requires that  $2\gamma_v < 1.6 \mu\text{rad}$  ( $49 \mu\text{m}$  at 30 m from the source). Hence, with cylindrical or spherical optics, submicron focusing at 3 mrad glancing angle is only practical with an  $\sim 1.3 \times 10^3 \mu\text{m}^2$  beam (gain  $\sim 1.3 \times 10^3$ ). In contrast, with elliptical mirrors and the same object distance and magnification, a practical K-B mirror system with less than  $0.5 \times 0.5 \mu\text{m}^2$  beam can be fabricated with a collection of  $\sim 2.5 \times 10^4 \mu\text{m}^2$  (gain  $\sim 10^5$ ).

The deposition profile required to modify a cylindrical mirror into an elliptical mirror is easily determined from the ideal surface figure of a focusing ellipse and the figure of the cylindrical approximation. For example, in Fig. 3 we plot the surface profile of an ideal ellipse with  $F_1 = 30$  m,  $F_2 = 0.06$  m, and  $\theta = 0.003$ . This profile is compared with the profile for its cylindrical approximation. The difference between the two profiles is also plotted in Fig. 3, offset by  $0.7 \mu\text{m}$ . This deposition profile will modify the cylindrical approximation and turn it into an ideal elliptical surface.

For a real mirror, the deposition process can also be used to correct small deviations from the nominal cylindrical figure. For example as shown in Fig. 4 (bottom line), the deviations of a typical 90 mm long substrate from its design cylindrical approximation are on the order of  $\pm 3 \mu\text{rad}$  with a rms slope error of  $1.7 \mu\text{rad}$ . The long period deviations in slope can be corrected (top curve) with the potential of reducing the residual rms slope errors to less than  $0.5 \mu\text{rad}$  as shown.

## III. FABRICATION AND ALIGNMENT TOLERANCES

### A. Surface roughness

Short-length-scale variations from an ideal mirror surface are referred to as “surface roughness.” The surface roughness required for efficient mirrors can be estimated

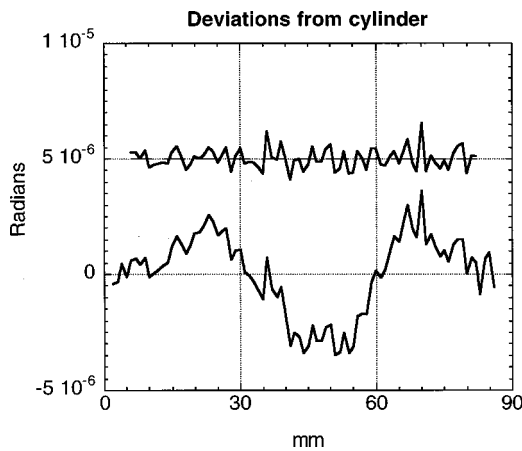


FIG. 4. Bottom curve shows residual slope errors in a nominal 90 mm long cylindrical mirror. If the low frequency slope errors are removed, the high frequency slope errors have a much lower rms deviation from an ideal cylinder (top curve displaced by 5  $\mu$ rad).

from the fraction of the reflected power contained in the geometrical image. The total intensity into the geometrically demagnified beam is approximated by

$$I = I_0 \exp\left(\frac{-4\pi\theta\sigma_s}{\lambda}\right)^2. \quad (3)$$

Here  $\sigma_s$  is the rms surface roughness below spatial frequencies of  $\sim 1$  cm and  $\theta$  is the mirror angle.<sup>4</sup> For 90% power into the geometrical image and with  $\theta = 3$  mrad, the surface roughness below 1 cm must satisfy  $\sigma_s < 8.6\lambda(\text{\AA})$ . With a typical operational energy of 20 keV this corresponds to  $\sigma_s < 5(\text{\AA})$ .

**B. Surface figure**

Long-length-scale deviations from an ideal mirror surface are referred to as figure errors. The required surface figure precision can also be set by a simple estimate. Image blur due to the slope errors depends on the focal length of the mirror and the rms slope errors;  $b = 2F_2\sigma_s$ , where  $\sigma_s$  is the rms slope error. For a focal length of 0.13 m, and a desired rms focal-spot size of less than 0.5  $\mu$ m, this corresponds to a rms slope error of  $\sim 2$   $\mu$ rad. Note to achieve a FWHM Gaussian focus below 0.5  $\mu$ m requires a submicroradian rms slope errors for this focal length. For shorter focal length optics (i.e., horizontal K-B mirror), the required figure perfection is relaxed.

**C. Object distance**

One concern with a monolithic focusing system is that the device may only be useable on a particular beamline. We note that an ideal microfocusing elliptical mirror works well over a wide range of object distances. Locally the radius of curvature is given by

$$R = \frac{2F_1F_2}{(F_1 + F_2)} \sin \theta. \quad (4)$$

Here  $F_1$  is the object distance,  $F_2$  is the image distance, and  $\theta$  is the mirror angle. As shown in Fig. 3, a local cylindrical approximation matches the slope of the ideal ellipse

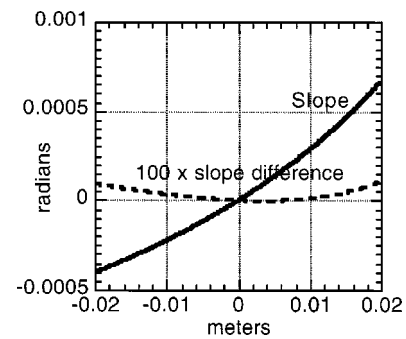


FIG. 5. Comparison of the slopes for elliptical mirrors with identical image distances and angles ( $F_2 = 0.06$  m,  $\theta = 0.003$ ), but with different object distances  $F_1 = 10$  and 30 m. The difference is shown multiplied by a factor of 100 for clarity.

over a small region, but deviates as the useful aperture of the mirror increases. For  $F_1$  large compared to  $F_2$  the local radius is approximated by  $R = 2F_1 \sin \theta$ ; hence, the object distance has only a secondary impact on the figure. For example, the ideal slopes for two elliptical mirrors with identical properties except for their object distances (10 and 30 m) are compared in Fig. 5.

**D. Image distance**

Whereas the object distance can be easily adjusted, the image distance must be held to tolerances of less than about 2%. As shown in Fig. 6, an error of 2 mm in the image distance for a nominal 60 mm focal length mirror (3%) restricts the useful aperture of the mirror to about 75% of the range necessary to collect a 1 mrad focused beam.

**E. Scattering angle**

The angular precision with which the mirrors must be adjusted can be estimated from the mirror aperture and the desired spot size. For example, a typical microfocusing mirror with 100  $\mu$ m aperture and a goal of less than 0.5  $\mu$ m image, must control the focal distance to 0.5%. For a 3 mrad glancing angle this corresponds to  $\sim 15$   $\mu$ rad. If the aperture is smaller, than the angular precision can be relaxed whereas larger aperture increases the required angular precision.

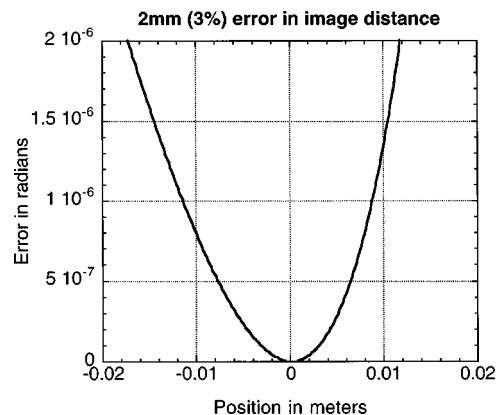


FIG. 6. Deviation between an ideal elliptical surface with 62 and 60 mm focal length and a nominal 3 mrad glancing angle. Note that the angle is adjusted slightly to minimize the deviations.

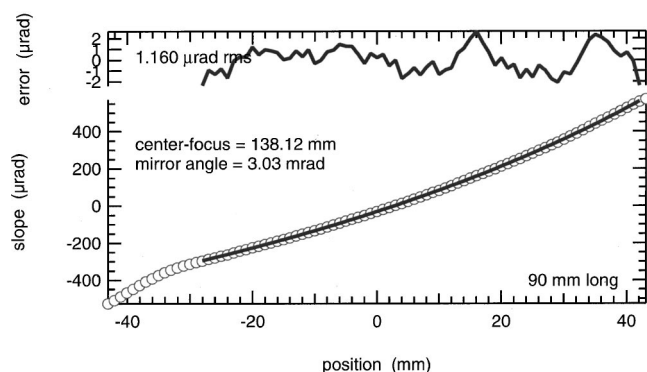


FIG. 7. Comparison of the ideal and actual figure for an elliptical surface. The rms deviation from the ideal elliptical fit ignoring the first 10 mm of the mirror is about  $1 \mu\text{rad}$ . The deviation from the ideal ellipse is even less over smaller regions of the mirror.

#### IV. MIRROR SUBSTRATE, DEPOSITION METHOD, AND METROLOGY

The mirror substrates were prepared at Beamline Technology Corporation (BTC) and differential depositions were performed in a dedicated differential deposition chamber. Small ultrasmooth spherical mirrors were prepared by polishing a large prediced Si plate. The large Si plate was divided into smaller mirror blanks by nearly cutting through the plate. The cuts were filled with hard wax and then the entire plate was optically and superpolished to achieve the desired spherical radius and surface roughness. By polishing a large plate, round-off errors at the edges of the individual mirrors were minimized. After superpolishing, the mirrors were separated and measured with a long-trace profile (see, e.g., Fig. 4). The long-trace profiler measurements were performed at the APS metrology laboratory where the estimated measurement uncertainty is  $<0.25 \mu\text{rad}$ .<sup>11</sup>

The differential deposition required to turn each cylindrical mirror into an ellipse was calculated from the theoretical elliptical and measured cylindrical slopes. Differential deposition was performed at BTC in a specially designed 1.5 m linear ultrahigh vacuum coater. Studies at BTC indicate that with proper care, and for  $\sim 1 \text{ \AA}$  rms roughness substrates, films as thick as  $3 \mu\text{m}$  can be deposited before a measurable increase in surface roughness can be detected. An initial binder coat of Cr is deposited. The mirror is then passed under a sputter source and the sputter source power is varied depending on the position of the mirror. The sputter power is limited to a small fraction of its range to ensure a linear deposition versus power dependence. For the K-B mirrors as many as 300 passes are required to achieve the desired elliptical figure. Because the overall mirror angle is adjustable, there is freedom to choose either a deposition profile where the deposition *gradient* is minimized at the center of the mirror, or a deposition profile where the maximum deposition *depth* is minimized. Better performance results with minimized gradient at the center of the mirror.

The required perfection of the deposition can be estimated from Eq. (2); the actual blur is proportional to the fractional deposition error times the uncorrected blur predicted by Eq. (2). Typically a deposition perfection of better than 5% is essential for high performance. A perfection of

1% is required to achieve a 100–200 nm image at the design focal length. After deposition, the mirrors were again measured with the APS long trace profiler (Fig. 7). Small smooth errors in deposition can be compensated by fitting the measured slopes to a general elliptical figure to determine the best fit mirror angle and focal length. The mirrors can then be mounted at focal lengths corresponding to their best fit positions.

We note that repeated depositions can be used to refine the surface figure and remove residual errors. For example, two depositions within  $\sim 10\%$  of the design deposition can in principle be used to achieve the desired 1% figure deposition accuracy.

The slopes from a typical deposition are compared in Fig. 7 to an ideal elliptical surface. Note that the edge effect over the first few millimeters of the mirrors can be corrected by more precise control of the sputter gun and the carriage.

#### V. OTHER CONSIDERATIONS

##### A. Intermediate slits

Slits can be used to relax the required geometrical demagnification when image size is more important than flux. For example, a slit between the object and the mirrors restricts the beam divergence and can also act as a new effective object. If the ratio of the slit size to its effective object distance is less than the ratio of the actual source size to its object distance, then the geometrical demagnification is improved by the slit. For example, ray tracing predicts that submicron focusing is possible with an  $\sim 720 \mu\text{m}$  source and for  $F_1 = 40$  and  $F_2 = 0.06$  m. With the addition of a  $100 \mu\text{m}$  slit, 10 m upstream of the mirror pair, the predicted focal spots size improves to  $0.25 \mu\text{m}$ . This predicted improvement can be understood in terms of focusing from the slit itself. Although the effective object distance is shorter, the effective object size is much smaller which allows for smaller final image size.

##### B. Windows and scattering sources

Windows and other scattering sources increase the beam emittance and degrade focusing performance by shortening the object distance and by increasing the effective object size. The number of windows should therefore be restricted, and they should be polished to minimize scattering.<sup>1</sup> For example, experience on the UNICAT beamline 33-ID and other beamlines has shown that the removal of graphite filters can greatly improve x-ray imaging with microfocusing optics.<sup>12</sup> The measurements reported in this article were performed with a standard APS graphite thermal filter associated with a so-called commissioning window. It is anticipated that focal spot size and efficiency can be improved by removing this conditioning window.

##### C. Scattering angle variation

Strongly demagnifying K-B mirrors include a significant variation in the x-ray scattering angle from one end of the mirror to the other. For x-ray microdiffraction it is useful to limit the beam divergence to less than  $\sim 1$  mrad. This sets

a limit on the scattering angle variation to about 0.5 mrad from one end of the mirror to the other. Hence, a mirror with a nominal scattering angle of 3 mrad has a scattering angle of 2.75 mrad on one end of the mirror and a scattering angle of 3.25 mrad on the other end of the mirror. This small variation in the scattering angle causes a gradient in the critical energy from one end of the mirror to the other with a total range of  $\sim 18$ – $21$  keV.

## VI. EXPERIMENTAL RESULTS

An x-ray microfocusing system based on differentially deposited mirrors has been fabricated and tested on the MHATT-Cat beamline 7-ID at the APS. The source is an APS type A undulator with source parameters described previously. The system used a 90 mm long primary mirror for focusing in the vertical plane and a 40 mm long secondary mirror for focusing in the horizontal (ring) plane. An L5 slit at 27 m was used to control the total power in the beam and to restrict the source size. The geometrically demagnified beams should have a FWHM of less than  $0.23 \times 0.22$  in the vertical and horizontal directions. However, slope errors add an additional blurring of about  $0.63$  (vertical)  $\times$   $0.3$  (horizontal) for  $1 \mu\text{rad}$  slope errors. Adding in quadrature the slope error blurring to the geometrical image we predict an image size of  $0.67$  vertical  $\times$   $0.38$  horizontal for  $1 \mu\text{rad}$  slope errors. The measured image size is in good agreement with this estimate and indicates that somewhat better than  $1 \mu\text{rad}$  slope errors are present for these mirrors. For best performance, only a fraction of the total mirror acceptance can be used because the deposition process is not yet precise enough over the entire mirror. With a  $50 \times 50 \mu\text{m}^2$  entrance aperture, beams as small as  $0.4 \times 0.5 \mu\text{m}^2$  have been measured. Example beam profiles are shown in Figs. 8(a) and 8(b).

## VII. DISCUSSION

As illustrated earlier, differential deposition can be used to produce small monolithic elliptical mirrors for x-ray microfocusing. Prototype mirrors already work well and the performance of future versions will continue to improve as the accuracy and precision of the deposition process improves. With increased object distances, smaller focal length designs and improved deposition precision, it appears practical to fabricate K–B optics with focal spots approaching  $0.1 \mu\text{m}$ .

The implications of the differential deposition techniques illustrated in this article go beyond microfocusing mirrors. In general, differential deposition offers a new direction for improving figure errors in virtually all x-ray mirrors. Although differential deposition was used to correct spherical errors in K–B mirrors, it can also be used to remove polishing errors for flats, spheres, and a spherical surfaces. Mirrors up to 1.5 m can be handled in the differential deposition chamber used for these studies. BTC has demonstrated the use of differential deposition for refiguring large mirrors where figure errors approaching  $1 \mu\text{rad}$  have been achieved. This new direction offers greater freedom in mirror design and fabrication.

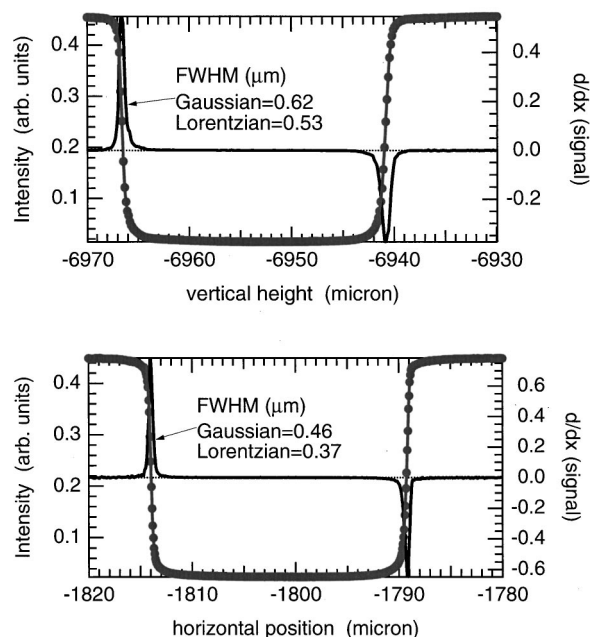


FIG. 8. Measured upper limit to the horizontal and vertical focal spot size. In these measurements the spot size is determined by taking the derivative (Gaussian) of the transmitted intensity (square wave) recorded as a  $22 \mu\text{m}$  diameter Au coated Pt wire is passed in front of the beam. The actual focus is in fact slightly smaller than the measured due to edge effects at the wire.

## ACKNOWLEDGMENTS

Research sponsored by the Division of Materials Sciences, U.S. Department of Energy under Contract No. DE-AC05-96OR22464 with Lockheed Martin Energy Research. Research in part on MHATT-Cat beamline 7 at the APS funded through the U.S. Department of Energy, Basic Energy Science. Metrology performed at the Advanced Photon Source Metrology Laboratory supported under Contract No. W-31-109-ENG-38 with the Department of Energy.

- <sup>1</sup>G. E. Ice, *X-Ray Spectrom.* **26**, 315 (1997).
- <sup>2</sup>P. Kirkpatrick and V. Baez, *J. Opt. Soc. Am.* **38**, 766 (1948).
- <sup>3</sup>J. H. Underwood, A. C. Thompson, Y. Wu, and R. D. Giaque, *Nucl. Instrum. Methods Phys. Res. A* **266**, 296 (1988); Y. Wiu, A. C. Thompson, J. H. Underwood, R. D. Giaque, K. Chapman, M. L. Rivers, and K. W. Jones, *ibid.* **291**, 146 (1990).
- <sup>4</sup>A. K. Freund, F. de Bergeuin, G. Marot, C. Riekel, J. Susini, L. Zhang, and E. Ziegler, *Opt. Eng.* **29**, 928 (1990).
- <sup>5</sup>P. J. Eng, M. Newville, M. L. Rivers, and S. Sutton, *Proc. SPIE* **3449**, 145 (1998).
- <sup>6</sup>H. A. Padmore, M. R. Howells, S. Irick, T. Renner, R. Sandler, and Y.-M. Koo, *Proc. SPIE* **2856**, 145 (1996).
- <sup>7</sup>Z. Cai, W. Yun, and P. Plag, *Proc. SPIE* **2516**, 52 (1996).
- <sup>8</sup>A. K. Freund, European Synchrotron Radiation Facility, Grenoble, France (private communication) (1999).
- <sup>9</sup>M. R. Howells and J. B. Hastings, *Nucl. Instrum. Methods Phys. Res.* **208**, 379 (1983).
- <sup>10</sup>See for example, G. K. Shenoy, P. J. Viccaro, and D. M. Mills, *Characteristics of the 7 GeV Advanced Photon Source: A Users Guide*, ANL-88-9 (Argonne National Laboratory, Argonne, IL); for current emittance and coupling <http://www.aps.anl.gov/aod/mcrops/gifs/beamproperties.html>
- <sup>11</sup>P. Z. Takacs, E. Church, L. Church, C. Bresloff, and L. Asoufid, *Appl. Opt.* **38**, 5468 (1999).
- <sup>12</sup>Bennett Larson, Oak Ridge National Laboratory, Oak Ridge, TN (private communication) (1999).